Title

Soluble adenylyl cyclase coordinates intracellular pH homeostasis and biomineralization in calcifying cells of a marine animal

Journal

American Journal of Physiology - Cell Physiology, 324(3)

ISSN

0363-6143

Authors

Chang, William Weijen
Thies, Angus B
Tresguerres, Martin
et al.

Publication Date

2023-03-01

DOI

10.1152/ajpcell.00524.2022

Soluble adenylyl cyclase coordinates intracellular pH homeostasis and biomineralization in calcifying cells of a marine animal

William W. Chang (張維仁)[1], Angus B. Thies[2], Martin Tresguerres[2], Marian Y. Hu (胡永安)[1]

[1]Institute of Physiology, Christian-Albrechts-Universität zu Kiel, Kiel 24118, Germany
[2]Scripps Institution of Oceanography, UC San Diego, CA 92093, USA

Abstract

Biomineralizing cells concentrate dissolved inorganic carbon (DIC) and remove protons from the site of mineral precipitation. However, the molecular regulatory mechanisms that orchestrate pH homeostasis and biomineralization of calcifying cells are poorly understood. Here we report that the acid-base sensing enzyme soluble adenylyl cyclase (sAC) coordinates intracellular pH (pH_i) regulation in the calcifying primary mesenchyme cells (PMCs) of sea urchin larvae. Single cell transcriptomics, *in situ* hybridization, and immunocytochemistry elucidated the spatial-temporal expression of sAC during skeletogenesis. Live pH_i imaging of PMCs revealed that down-regulation of sAC activity with two structurally unrelated small molecules inhibited pH_i regulation of PMCs, an effect that was rescued by addition of cell-permeable cAMP. Pharmacological sAC inhibition also significantly reduced normal spicule growth as well as spicule regeneration, establishing a link between PMC pH_i regulation and biomineralization. Finally, increased expression of sAC mRNA was detected during skeleton re-mineralization and during exposure to CO_2-induced acidification. These findings suggest that transcriptional regulation of sAC is required to promote re-mineralization and compensate for acidic stress. The present work highlights a central role of sAC in

coordinating acid-base regulation and biomineralization in marine calcifying cells in times of rapid anthropogenic ocean acidification.

Keywords: primary mesenchyme cells, cAMP, calcification, ocean acidification, skeletogenesis

Introduction

The shells and skeletons of major marine calcifying animals are primarily comprised of calcium carbonate ($CaCO_3$) (1). The required CO_3^{2-} ions are obtained from seawater in the form of HCO_3^- or by the hydration of metabolic CO_2 (2). Accordingly, CO_3^{2-} precipitation releases H^+ that must be promptly removed from the site of biomineralization to protect pH homeostasis and sustain high biomineralization rates. Indeed, pH regulation and biomineralization are intrinsically linked in all calcifying invertebrates including corals (3), molluscs (4), brachiopods (5) and echinoderms (6). Moreover, this principle also applies to the inner ear of teleost fish and their otoliths (7), to mammalian teeth (8), and even to calcifying phytoplankton (9). However, the mechanisms that coordinate acid-base relevant ion transport and biomineralization are not completely understood, especially at the molecular and cellular level.

The sea urchin larva develops an elaborate endoskeleton composed of magnesium-rich calcite. Radioisotopic labelling using ^{14}C demonstrated that about 60% of the dissolved inorganic carbon (DIC) used for skeletogenesis derives from metabolic CO_2 while the remaining 40% is absorbed from seawater (2). Biomineralization is initiated by the formation of amorphous calcium carbonate (ACC) within vesicles of the calcifying primary mesenchyme cells (PMCs) (10). These cells form syncytial cables that surround the endoskeleton and are proposed to exocytose ACC to the growing spicule where the crystallization of calcite takes place (11). During this process, each mole of CO_3^{2-} that is precipitated generates 1.6 moles H^+, which need to be removed to protect PMCs from

acidification. This requires cellular proton export rates that are comparable to those of acid-secreting osteoblasts, parietal and renal tubular cells (12). Accordingly, PMCs express a suite of acid-base relevant ion transporting proteins including Na^+/HCO_3^- cotransporter (NBC) (6, 13, 14), Na^+/H^+-exchanger (NHEs), V-type H^+-ATPase (VHA) (6), and the H^+-selective channel Otopetrin (Otop2L) (15). Gene expression analyses and live cell experiments combined with pharmacological and genetic knock-down revealed that NBC (Sp-Slc4a10) together with the extracellular carbonic anhydrase Cara7 is the main pathway for DIC uptake (16), and that Otop2L plays a central role in H^+ removal from the cell (15). The existence of diverse acid-base transporters in PMCs implies the need to dynamically adjust DIC and H^+ transport in PMCs to match biomineralization rates.

The soluble adenylyl cyclase (sAC; *adcy10*) has been demonstrated to coordinate cellular ion-transport in acid-base regulatory epithelia and calcifying cells of marine organisms (17–19). This enzyme is stimulated by HCO_3^- to produce the ubiquitous messenger molecule cyclic adenosine monophosphate (cAMP), and in association with carbonic anhydrases (CAs), sAC can also act as a CO_2 and pH sensor (20). Given its presence in diverse organisms ranging from cyanobacteria to mammals, sAC has been deemed an evolutionarily conserved acid-base sensor (21, 22). The role of sAC as a molecular acid-base sensor seems especially prominent in aquatic organisms, perhaps due to their relatively low buffering capacity and ensuing large acid-base disturbances from metabolic and environmental origins (23, 24). The role of sAC is best characterized in fish gill ionocytes where it contributes to blood acid-base homeostasis (19, 25–27). The sAC-dependent mechanism is independent from any autocrine or paracrine regulation; instead, sAC senses the acid-base status inside each gill ionocyte and triggers the activation of VHA to transport H^+ from the cell into the blood (19, 25) and, potentially, the activation of anion exchangers to excrete HCO_3^- into seawater (23, 28). Furthermore, sAC-dependent modulation of VHA has been reported in mammalian

epididymis (29) and kidney (30), suggesting a universal sensor-effector coupled mechanism in acid-base regulatory epithelial cells. Additionally, sAC has been implied to regulate intestinal carbonate precipitation in marine fish (20, 31), otolith formation in the fish inner ear (17), and coral skeletal formation (18). In the latter, the functional role of sAC was evidenced by reductions of both the pH of the extracellular calcifying medium located in between the calcifying cells and the skeleton and in the skeletal deposition rate upon pharmacological application of the sAC-specific small molecule inhibitor KH7 (18). After rat, mouse, and human (32), sea urchin was the first animal in which sAC was found and a physiological function characterized (33). Like in many other animals, sea urchin sAC ($_{su}$sAC) modulates sperm motility and the acrosome reaction (33, 34) but information regarding a function of this enzyme in the calcifying PMCs remains unknown. Thus, the present study investigates a potential role of $_{su}$sAC in coordinating PMC pH_i regulation and skeletal formation (35). First, we examined the presence of $_{su}$sAC mRNA and protein in PMCs. Next, we determined the role of $_{su}$sAC in PMC pH_i regulation through live cell imaging experiments using the pH-sensitive ratiometric dye BCECF-AM and two structurally unrelated small molecules that specifically inhibit sAC, KH7 and TDI-8164, respectively. Finally, we explored the functional role of $_{su}$sAC in skeletal formation through biomineralization assays in control, re-biomineralizing, and ocean acidification (OA)-exposed sea urchin larvae. Overall, the results established a role of sAC in coordinating pH_i regulation and biomineralization in sea urchin larvae.

Results and Discussion

Identification and localization of $_{su}$sAC expression in the developing sea urchin larva

Phylogenetic analysis demonstrated that $_{su}$sAC forms a clade with sAC orthologues from other invertebrates ranging from sponges over molluscs to basal

deuterostomes. This sAC clade of invertebrates formed a separate branch from vertebrate sACs (Figure 1A). Single-cell transcriptomics were applied to analyze spatiotemporal expression of $_{su}$sAC mRNA in mesenchyme blastula (24 hpf), late gastrula (40 hpf), and pluteus (72 hpf) larvae (Figure 1B). Specification of the calcifying primary mesenchyme cells (PMCs) takes place during mesenchyme blastula (36). At this stage, $_{su}$sAC mRNA expression was already evident in a few PMCs (Figure 1B). During late gastrulation $_{su}$sAC mRNA was primarily expressed in the PMC cluster that is associated with the initiation of spiculogenesis (Figure 1B). The pluteus larval stage is characterized by spicule extension (36) and also in this stage $_{su}$sAC mRNA expression was highest in PMC clusters of the post-oral tips and in the middle section of the body rods (Figure 1B). Lower expression levels of $_{su}$sAC were detected in the gut and ectodermal cells. These results were supported by *in situ* hybridization of $_{su}$sAC with an antisense probe targeting to the catalytic domain sequence (Figure 1C). Along the first days of development gene expression analyses detected a steep decrease in $_{su}$sAC mRNA levels between 1-5 dpf (Figure 1D). This observation stands in contrast to a previous study had reported a steep increase in $_{su}$sAC mRNA abundance in the initial hours post fertilization peaking at the gastrula to prism stage where development of the gut and skeleton is initiated (35). We repeated these experiments to confirm our measurements and think that differences between these studies may drive from the selection of different housekeeping genes or from the use of primers targeting different domains of the sAC gene. The PMC developmental gene regulatory network is well studied, and the regulatory transcription factors Alx1 and Ets1 are essential for the specification of calcifying primary mesenchyme cells prior to mesenchyme ingression and subsequent skeletogenesis (37, 38). Interestingly, $_{su}$sAC mRNA levels are significantly decreased in Alx1 morphants but not in Ets1 morphants (Figure. S1). This suggests that $_{su}$sAC mRNA expression is under Alx1 control, and that downstream $_{su}$sAC activity is required for the proper functionality of the calcifying PMCs.

The sAC gene is characterized by extensive alternative splicing resulting in multiple protein isoforms with diverse structural domains and regulatory properties (39). In mammals, the most active sAC isoform is truncated sAC (sAC_T), a ~48 kDa protein comprised of the two catalytic domains that are both essential for HCO_3^--stimulated cAMP-production (32). Here, we found sea urchin larvae predominantly express a ~45 kDa truncated sAC protein ($_{su}sAC_T$) (Figure 2A). The anticipated size of full-length $_{su}$sAC is ~209 kDa, and the predicted peptide size of $_{su}$sAC catalytic domains is ~ 56 kDa. Although this predicted peptide is larger than what we detected by our westen blot analysis, it is very likely that alternative splicing produces the $_{su}sAC_T$ of 48 kDa. Such splice variants were also frequently described in the vertebrate sAC systems (40, 41) but remain unresolved for the $_{su}$sAC. Whole mount immunostaining revealed high $_{su}sAC_T$ protein abundance in PMCs, and presence in ectodermal epithelial and cells of the ciliary bands (Figure 2 B-E). High resolution 3D reconstructions from airyscan confocal z-stacks demonstrated that $_{su}sAC_T$ is present in the cytoplasm of PMCs including the syncytial cable (Figure 2 F, G). These molecular and immunological analyses provide evidence for the presence of $_{su}$sAC, likely as a truncated form only consisting of the catalytic C1-C2 domains in calcifying cells of the sea urchin larva.

Role of $_{su}$sAC in PMC pH_i regulation

To specifically look at the role of $_{su}$sAC in PMC pH_i regulation, we performed live cell imaging experiments in combination with the NH_4Cl pre-pulse technique to measure the ability of PMCs recovering from an induced acidosis (Figure 3). We have extensively used this technique to assess acid-base regulatory mechanisms in PMCs based on their pH_i recovery rate (6, 15), and here we performed similar experiments in the presence of two sAC-specific pharmacological inhibitors.

The first inhibitor, KH7, decreased PMC pH_i recovery in a dose-response manner (IC_{50} ~2 μM) (Figure 3A, B). At the highest KH7 concentration (40 μM), PMC pH_i recovery was significantly decreased to half of that seen in DMSO-treated controls (0.06 ± 02 vs 0.12 ± 0.02 pH units min^{-1}, respectively). Rescue of KH7-induced inhibition of pH_i recovery by db-cAMP (0.15 ± 0.01 pH units min^{-1}) confirmed the involvement of $_{su}$sAC (Figure 3C, D). The second sAC inhibitor, TDI-8164, had identical effects on PMC pHi recovery, namely, significant inhibition compared to controls and full rescue by db-cAMP (respectively, 0.09 ± 0.03, 0.13 ± 0.03, and 0.15 ± 0.04 pH units min^{-1}) (Figure 3E, F). Other than genetic knockdown, which is not possible in this case due to the role of sAC in gastrulation (35), comparable inhibition by two structurally unrelated pharmacological inhibitors and rescue of the resulting phenotype by cAMP is the strongest possible evidence for the involvement of $_{su}$sAC in sea urchin larva PMC pH_i regulation.

$_{su}$sAC is required for biomineralization under control and acidified conditions

In a next step we looked at the effect of pharmacological down-regulation of sAC activity on sea urchin larvae biomineralization. To prevent an off-target effect on gastrulation (35), KH7 was applied at the late gastrula stage (1.5 dpf) where skeletal development begins. Tracking spicule growth in 2 to 4 dpf larvae demonstrated a dose-dependent decrease in the biomineralization rate of the growing spicules from 80.46 ± 13.94 μm day^{-1} in control larvae down to 36.99 ± 4.37, 25.14 ± 5.89 and 20 ± 3.81 μm day^{-1} in larvae treated with 1, 2 and 4 μM KH7, respectively (Figure 4 A, B).

To further disentangle potential collateral effects of KH7 on other developmental processes that could indirectly impair skeletogenesis, we performed a re-calcification assay with 3 dpf larvae. This experiment demonstrated that pharmacological $_{su}$sAC

inhibition induced a dose-dependent decrease in spicule re-biomineralization from 14.95 ± 3.61 µm day^{-1} down to 5.14 ± 1.23, 1.07 ± 1.26 and 0.5 ± 0.81 µm day^{-1} (1, 2 and 4 µM KH7) (Figure 4C). Re-calcifying larvae subsequently demonstrated roughly double the $_{su}$sAC mRNA levels compared to controls (Figure 4D). These results indicate that $_{su}$sAC activity is essential both for normal biomineralization and for re-mineralization following skeleton dissolution by an extreme acidic challenge.

Finally, we analyzed $_{su}$sAC mRNA expression in sea urchin larvae that had been exposed to control (pH 8.1, 400 µatm pCO_2), mild (pH 7.7, 1250 µatm pCO_2), and extreme (pH 7.5, 4000 µatm pCO_2) CO_2-induced seawater acidification between 0-5 dpf (14). These OA-exposed larvae were reported to experience reduced body length growth; however, they were able to biomineralize their skeletons at a rate that was comparable to controls (based on body size-specific Ca^{2+} accumulation) (14). Analysis of $_{su}$sAC mRNA levels by RT-qPCR in the same samples revealed significant ~two-fold upregulation in 2 dpf larvae exposed to the lowest pH treatment (Figure 4E), and whole mount *in situ* hybridization confirmed the presence of $_{su}$sAC mRNA in PMCs as well as in ectodermal and developing gut cells in larvae raised under acidified conditions (Figure 1B). These results provide a link between PMC $_{su}$sAC and compensatory responses to OA that maintain biomineralization during an environmentally relevant acidic challenge.

Conclusions

The various lines of evidence presented in the current study indicate that $_{su}$sAC is a molecular acid-base sensor that coordinates pH_i regulation and biomineralization in sea urchin larvae PMCs during both, normal conditions and acidic challenges. It has been demonstrated that during active mineralization, pHi of PMCs is increased due to an enhanced uptake of bicarbonate that is needed for the calcification process (6). In fact, this carbon concentration mechanism has been recently resolved demonstrating an

interaction between the extracellular carbonic anhydrase, Cara7, with the Na^+-dependent HCO_3^- cotransporter Sp_Slc4a10 (16). It has been demonstrated that HCO_3^- stimulates $_{su}$sAC and initiates cAMP production (34). Accordingly, we propose that this elevation of the cytosolic carbonate pool stimulates $_{su}$sAC to activate cellular proton export pathways (Figure 5). This is essential to maintain intracellular pH homeostasis during precipitation of $CaCO_3$ where large amounts of protons are liberated inside the cell.

However, the exact mechanisms that stimulate $_{su}$sAC activity in PMCs need to be confirmed experimentally and the subsequent downstream signaling pathways and effectors are an exciting topic of future investigation. Based on previous experiments (6, 14, 15), the most promising candidates include the Na^+/HCO_3^- cotransporter (Sp_Slc4a10), Na^+/H^+-exchanger (Sp_Slc9a2) and the proton channel Otop2l; additionally, regulation of Na^+/K^+-ATPase cannot be ruled out (Figure 5). For example, sAC in rat cardiomyocytes is stimulated by HCO_3^- that enters the cell *via* Slc4 (42), a mechanism that may also take place in hagfish and lamprey (43). Interestingly, Slc4-stimulated sAC activity promotes, *via* protein kinase A (PKA), the transport of Ca^{2+} into the rat cardiomyocyte cytosol and sarcoplasmic reticulum (44). Thus, it is possible that $_{su}$sAC in PMCs simultaneously regulates the activity of multiple acid-base and Ca^{2+} transporters to ultimately coordinate pH_i and biomineralization.

A comparative analysis reveals striking similarities in the molecular machinery of diverse biomineralizing cells. In addition to sea urchin larva PMCs, Slc4 family Na^+/HCO_3^- cotransporters are also present in the calicoblastic cells that make the coral skeleton (45, 46), the ameloblasts that produce dental enamel (47), and matrix vesicles of human osteoblast-like cells (48). Analogous to NBC, sAC activity promotes biomineralization in sea urchin PMCs (this study), coral calcifying cells (49), fish inner ear epithelial cells that make the otoliths (17) as well as mammalian osteoblasts (50, 51) and ameloblasts (47). The strong association of sAC with biomineralizing systems

points towards a conserved physiological role of this enzyme in marine calcifying organisms. Here the sAC mediated activity between pH_i regulation and biomineralization should be more prominently considered when assessing potential effects of environmental disturbances on the vulnerability or resilience of marine organisms, and the assumptions used to reconstruct Earth's climates based on skeleton-bound proxies.

Material and Methods

Experimental animals

Adult purple sea urchins (*Stongylocentrotus purpuratus*) were collected in La Jolla (CA, USA) and shipped to the Helmholtz Centre for Ocean Research GEOMAR (Kiel, Germany). Animals were maintained in a recirculating seawater system (10°C, pH 8.1) 12/12 h light/dark cycle); fertilization and larval cultures were performed as previously described (13, 52). At various days post fertilization (dpf), larvae were collected for gene expression, pH_i regulation, and skeletal development analyses. The re-mineralization experiments involved exposing 3 dpf larvae to filtered seawater (FSW) with pH 6.0 [adjusted with 0.03 M 2-(N-morpholino) ethanesulfonic acid (MES)] for 12-15 hours (53). After dissolution of the skeleton, the larvae were transferred back to FSW (pH 8.1) to re-calcify their skeletons for 3-4 days; during this period, samples were collected daily for gene expression and skeletal development analyses. cDNA samples for gene expression analyses of larvae exposed to control and CO_2-acidified seawater were obtained from a previous study (14). The exposures were conducted in FSW bubbled with CO_2 to achieve (1) pH 8.1, 400 µatm pCO_2; (2) pH 7.7, 1250 µatm pCO_2, and (3) pH 7.5, 4000 µatm pCO_2.

At Scripps Institution of Oceanography, adult sea urchins were maintained in a flow-through seawater system (12°C, pH~8.0, 12/12 h light/dark cycle; fertilization was

performed as previously described (35). Larvae were raised for 3.5 days in constantly stirred FSW at 12°C before Western blotting or immunocytochemistry procedures.

Bioinformatics, RT-qPCR, and whole-mount in situ hybridization

The protein sequence of sea urchin soluble adenylylcyclase (sAC) (NP_001020380) was blasted to the NCBI database (https://www.ncbi.nlm.nih.gov), and sAC homologous with 0 E-value plus four mammalian homologous (E-value $e^{-114\sim-110}$) were selected for phylogenetic analysis. Selected sequences were processed through MUSCLE alignment and trimmed using Gblocks Server (http://molevol.cmima.csic.es/castresana/Gblocks_server.html). The Maximum Likelihood tree was generated by MegaX (54) with the best fit model LG+G and 500 bootstrap replicates.

Quantitative reverse transcriptase PCR (RT-qPCR) and cloning were performed as previously described (14). Gene expression levels were normalized to the reference gene *ef1α* (LOC548620), which is stable during normal larval development and during re-biomineralization (6). Whole-mount *in situ* hybridization was performed as previously described (14). The primers used for RT-qPCR and the probes used for *in situ* hybridization are listed in Table S1.

Single-cell transcriptomics

Single cell transcriptomics was performed as recently described (15) on larvae raised under control conditions at mesenchyme blastula (one day post fertilization, 1 dpf), late gastrulation (2 dpf), and pluteus (3 dpf) stages. Briefly, embryonic/larval cells were gently dissociated by pipetting until reaching >95% single-cell suspension (55). Dissociated single cells were washed twice in calcium-free seawater (CFSW), checked for viability (>95%) by propidium oodine staining, fixed in 90% ice-cold methanol, and stored at −20 ℃. Cells were re-hydrated in a descending methanol series and processed according to Single cell 3′ Reagent Kits version 3 user guide (10xGenomics).

Sequencing of libraries was performed on an Illumina Hiseq system resulting in an average of 23.015 raw reads per cell barcode (Illumina, San Diego, CA, USA). Raw reads were demultiplexed, aligned to *S. purpuratus* genome 5.0 (retrieved from Echinobase) (56) and counted using the CellRanger pipeline from 10xGenomics (version 3.0.2). Basic uniform manifold approximation and projection (UMAP) dimensional reduction and clustering was performed using the Seurat version 3.2 workflow (57, 58). Expression of $_{su}$sAC mRNA levels in control and in morphants for Alx1 were analysed from data generated in (37) using the NCBI SRA BLAST service.

Western blotting

S. purpuratus larvae (~25 mg) were added to 250 µL of 2X Laemmli Buffer (Bio-Rad, Hercules, CA, USA) with 5% (v/v) β-mercaptoethanol. Larvae were homogenized via gentle pipetting and 20 sec of sonication on ice prior to denaturing at 95°C for 5 min. Larval homogenate (32.4 µg) was loaded into a SDS/PAGE gel. Following electrophoresis, proteins were transferred onto a PVDF membrane using a Mini Tans-Blot Cell (Bio-Rad) overnight. The PVDF membrane was incubated in blocking buffer [10% powdered fat-free milk in TBS-T (BB_{WB})] (1 h at room temperature on an orbital shaker), and then incubated anti-sAC antibodies (0.55 µg ml^{-1} in BB_{WB}) or peptide-preabsorbed anti-sAC antibodies (60x excess peptide in BB_{WB}) (4 h at room temperature on an orbital shaker). The PDVF membrane was washed (3 x 10 min in TBS-T) prior to incubation with goat anti-rabbit-HRP antibodies (Bio-Rad) (1:10,000 in BB_{WB}) (1 h at room temperature on an orbital shaker). The PVDF membrane was again washed (3 x 10 min in TBS-T) prior to development with ECL Prime Western Blot Detection Kit (GE Healthcare, Chicago, IL, USA) and imaging in a Chemidoc Imaging system (Bio-Rad).

Immunofluorescence

S. purpuratus larvae were fixed in 4% (v/v) paraformaldehyde in fixation buffer (0.2M NaCl, 0.06M EPPS, in FSW) on an orbital shaker (15°C, 20 min). Fixed larvae were washed in FSW (6 x 5 min), then in PBS (3 x 5 min) before incubation with blocking buffer [BB_{IHC}; 5% (w/v) bovine serum albumin in PBS] (1 h at room temperature). Next, larvae were incubated with either rabbit polyclonal anti-sAC antibodies (5.5 µg ml^{-1} in BB_{IHC}), peptide-preabsorbed anti-sAC antibodies (20x excess peptide in BB_{IHC}), or BB_{IHC} alone (overnight at 4°C on a rotator). The anti-sAC antibodies recognize a 14 amino acid peptide in the second catalytic domain of sAC from the coral *Acropora digitifera* (LPG**D**KHEDD**P**ARAL) (49), which is 86% identical to the matching region in $_{su}$sAC (LPG**Y**KHEDD**C**ARAL). Anti-sAC antibody and peptide were produced by Genscript Biotech (Piscataway, NJ, USA). Larvae were washed to remove unbound primary antibody (4 x 5 min in PBS), and incubated with goat anti-rabbit Alexa Flour 555 antibodies (4 µg ml^{-1} in BB_{IHC} containing 1 µg ml^{-1} DAPI to label DNA) (1 h at room temperature on an orbital shaker). After washing (4 x 5 min in PBS), larvae were mounted on a depression slide and imaged on a Zeiss AxioObserver Z1 microscope connected to a laser scanner equipped with 405 and 561 nm laser lines (Zeiss LSM 800 with Airyscan, Carl Zeiss AG). $_{su}$sAC and DAPI signals were visualized using goat anti-rabbit Alexa Fluor 555 (Invitrogen, Waltham, MA, USA) and DAPI stain (Invitrogen), respectively (Alexa Flour 555 – ex: 561 nm, em: 540-700 nm; DAPI – ex: 405 nm, em: 400-600 nm). 3D reconstructions of z-stacks were generated using Imaris 9.0 (Bitplane, Zurich, Switzerland). sAC and DAPI signals are presented using the false colours orange and blue, respectively, in all figures.

Intracellular pH (pHi) imaging

Measurements of pH_i were perfomed using the cell permeable pH-sensitive dye 2',7'-Bis-(2-carboxyethyl)-5-(and-6)-Carboxyfuorecein, Acetoxymethyl Ester (BCECF-AM) as previously described (12, 13). Intracellular acidosis was induced by a 20 mM

NH_4Cl pre-pulse in FSW followed by washout in FSW during which pHi recovery rate was determined based on the linear slope of the curve and expressed as pH units min^{-1}. The washout solutions contained either 0.1% DMSO (carrier control) or sAC-specific specific small molecule inhibitors, KH7 (20, 59) or TDI-8164 (60). KH7 was purchased from Merck (Kenilworth, NJ, USA), while TDI-8164 was a generous gift from Drs. Lonny Levin and Jochen Buck (Weill Cornell Medical College, USA). Both sAC inhibitors were dissolved in DMSO. Experiments to rescue sAC activity employed cell membrane permeable dibutyryl cAMP (db-cAMP) (Merck) (100 μM) in conjunction with 40 μM KH7 in the wash-out solution. Measurements were performed in an alternating mode between control and inhibitor treated larvae and five to nine larvae were measured for every experimental condition.

Skeletal development

To quantify skeletal development, control and re-biomineralizing larvae were fixed in 4% PFA in FSW and imaged on an inverted microscope (Zeiss, Axiovert A1) equipped with a Axio cam 105 camera as previously described (6, 15). Body rod length (a proxy for spicule growth) in 2-4 dpf larvae was measured and analyzed using the Zen 3.2 Blue (Zeiss) software. Growth rates were calculated based on the average daily increase in body rod length over the four-day period and expressed in μm day^{-1}. To test the role of sAC in biomineralization, larvae were incubated to control or re-calcifying conditions in the presence of 0.1% DMSO or various concentrations of KH7. Three independent replicates were performed for each inhibitor concentration in 6 well plates. From each well 40-166 larvae were analyzed, averaged and treated as one replicate leading to a final n = 3.

Statistical analyses

Prism 6 (GraphPad, San Diego, USA) was used to conduct all statistical analyses and generate all graphs. All data were normally distributed and passed equal variance tests (Levene test). The effects of pharmacological treatments on gene expression, calcification rate, and pHi regulation were performed using one-way ANOVA followed by Holm-Sidak post-hoc test. All data are presented as mean and error bars indicate the standard error of the mean (SEM).

Acknowledgements: We are grateful to Drs. Amro Hamdoun and Kate Nesbit (SIO-UCSD) for providing sea urchin specimens, and Drs. Lonny Levin and Jochen Buck (Weill Cornell Medical College) for providing TDI-8164. The authors further thank, F. Thoben and and R. Lingg for maintenance of the sea urchin culture systems. **Funding:** M.Y.H. and W.W.C. are funded by the Emmy Noether Program (403529967) of the German Research Foundation (DFG). This work was partially supported by NSF Graduate Research (GRFP 2019271478), SIO Doctoral Scholar, and ARCS Fellowships to A.B.T., NSF grant #1754994 to M.T.

Figures and legends

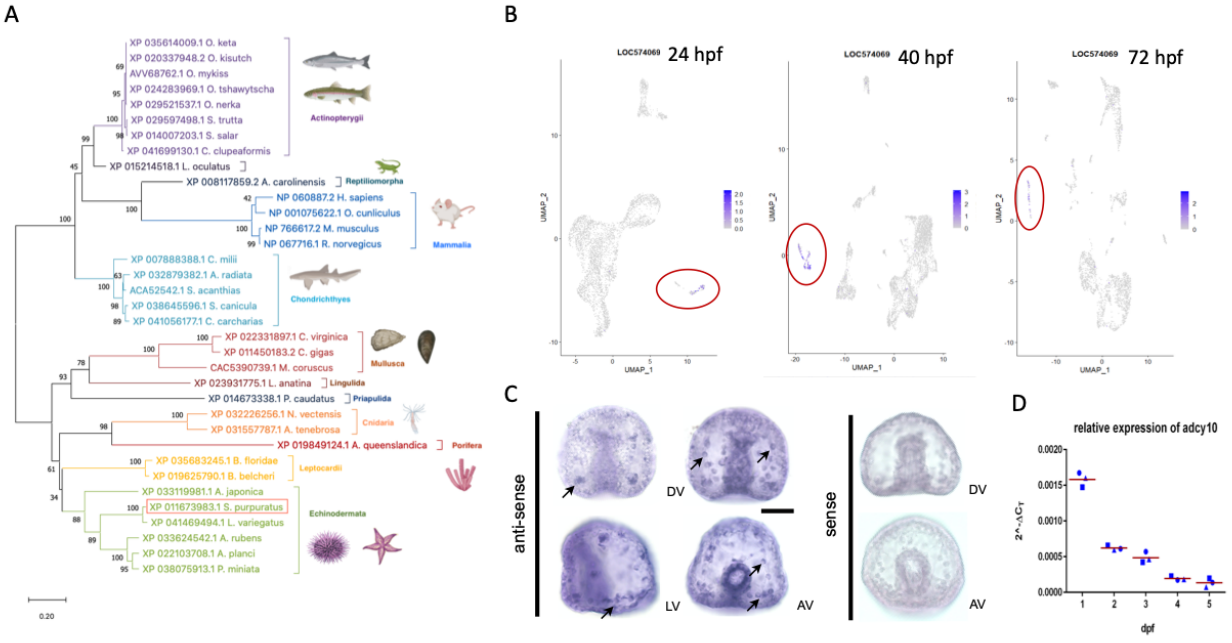

Figure 1 Phylogenetic analysis and expression of $_{su}$sAC in the developing sea urchin larva. (A) 34 homologous of $_{su}$sAC, including invertebrates and vertebrates, were blasted and filtered from NCBI database to generate a Maximum Likelihood tree. Bootstrap values of the branches were marked on the nodes. The branch lengths are proportional to the amino acid divergence per site (see scale bar). (B) Principle component analysis of single cell-RNA-seq results from 24, 40, and 70 hpf larvae. Clusters were annotated based on overlaps between cluster-enriched peaks of $_{su}$sAC (*adcy10*) and genes with known cell-specific activity. Normalized counts of *adcy10* are labeled from light blue to dark blue with increasing expression levels. PMC cluster is indicated by red oval. (C) *In situ* hybridization of *adcy10* in 2 dpf larvae cultured under hypercapnic conditions of pH 7.5. An antisense probe targeting to *adcy10* catalytic

domain sequence was applied to the hybridization, and a sense probe served as negative control. Arrows indicate the PMCs with positive *adcy10* signals. Abbreviations: dorsal view (DV), anal view (AV), lateral view (LV). scale bar = 50 μm. (D) The developmental mRNA expression level of *adcy10* from 1 dpf larvae to 5 dpf larvae.

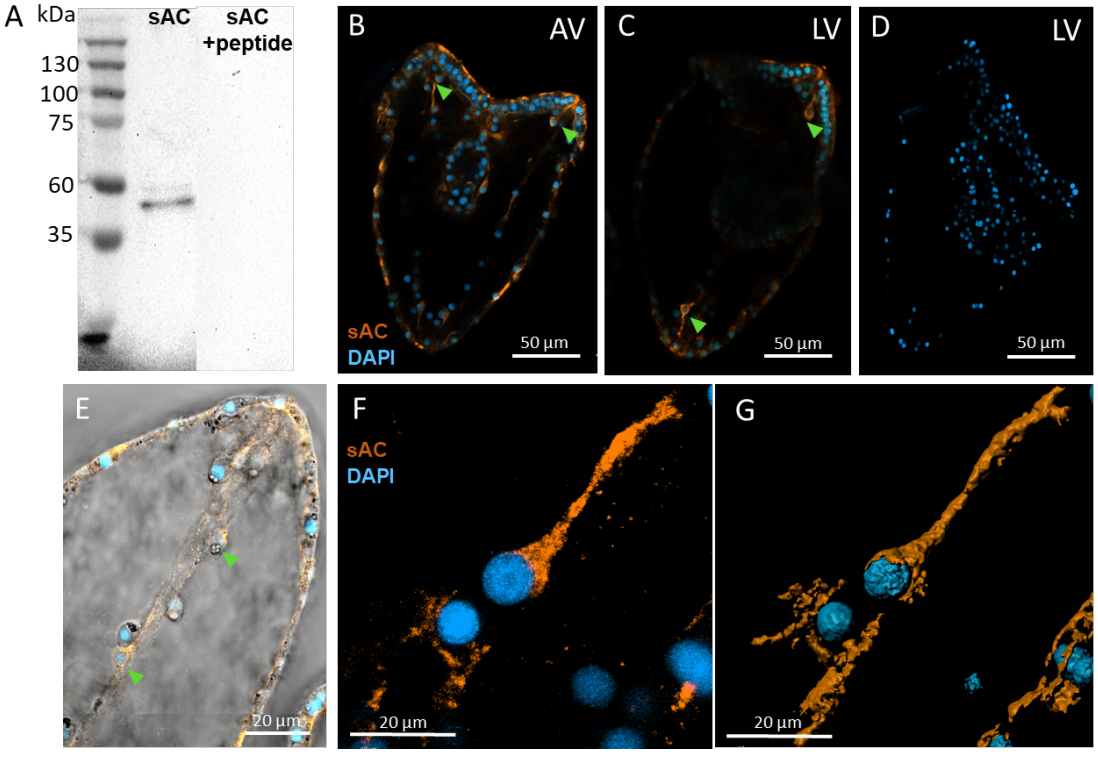

Figure 2 Immunocytological analyses of sAC in the sea urchin larva.

(A) Western blot analysis using the anti-coral sAC antibody against crude protein extracts of sea urchin-larvae. The right lane shows the blotting result using the primary antibody pre-absorbed with the immunization peptide. (B, C) Immunolocalization of $_{su}$sAC in 3 dpf sea urchin larva. Pseudocolors were applied on signals of sAC protein (orange) and nuclei (blue). $_{su}$sAC-positive PMCs were indicated by arrowhead. Abbreviations: anal view (AV), lateral view (LV). (D) Negative control without addition of the primary antibody. (E) Merged image of sAC immunostaining and bright field. $_{su}$sAC (orange); nuclei (blue). $_{su}$sAC-positive PMCs attaching to spicule were indicated by arrowhead. (F) Reconstituted 3D image of $_{su}$sAC staining. $_{su}$sAC (orange); nuclei (blue). The $_{su}$sAC signal followed the shape of PMC syncytial cables and is highlighted in (G).

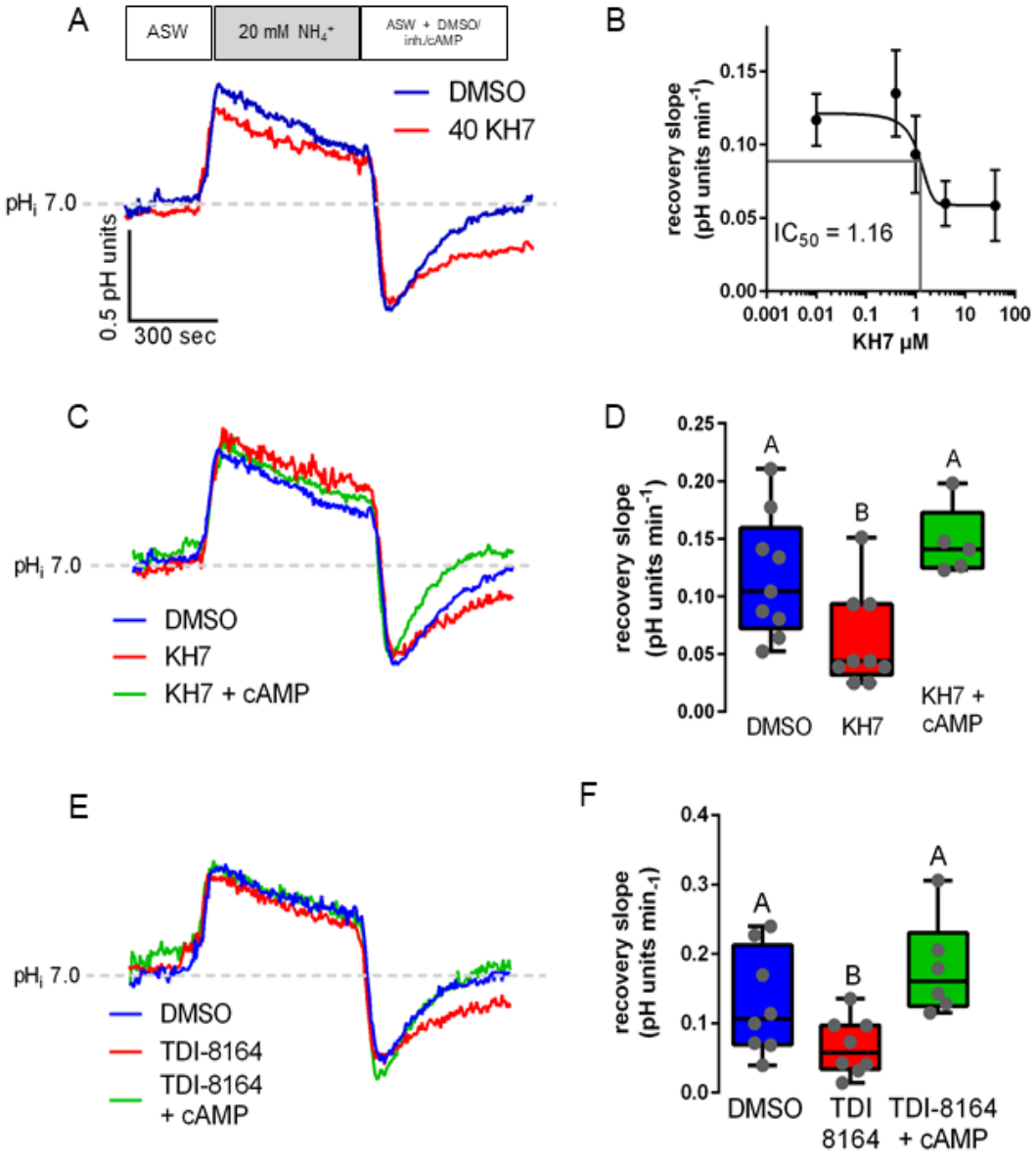

Figure 3 Effects of sAC activity on pH regulatory capacities of PMCs. (A) Average traces from real-time intracellular pH recordings in PMCs under control conditions (blue line) or in the presence 40 µM KH7 (red line). (B) Dose-dependency of recovery slopes under different doses of KH7 treatments (0.04

μM, 0.4 μM, 1 μM, 4 μM, and 40 μM). IC_{50} of KH7 on PMC pH_i regulation is 1.16 μM. (C) PMCs pH_i regulatory capacities in the presence of DMSO (blue line), 40 μM KH7 (red line), or 40 μM KH7 + 100 μM Dibutytyl cAMP (green line). (D) Average slope of PMC pH_i capacities at the given pharmacological treatment including control (blue box), sAC inhibition (red box), cAMP rescue (green box). (E) Real-time trace of pH_i regulatory capacities of PMCs that were treated with DMSO (blue line), 40 μM TDI-8164 (red line), or 40 μM TDI-8164 + 100 μM Dibutytyl cAMP (green line). (F) Average slopes of pH_i recovery in PMCs treated with DMSO (blue box), TDI-8164 (red box), and TDI-8164 + Dibutytyl cAMP (green box). N = 5-9, One-way ANOVA: $P<0.05$, Turkey's test.

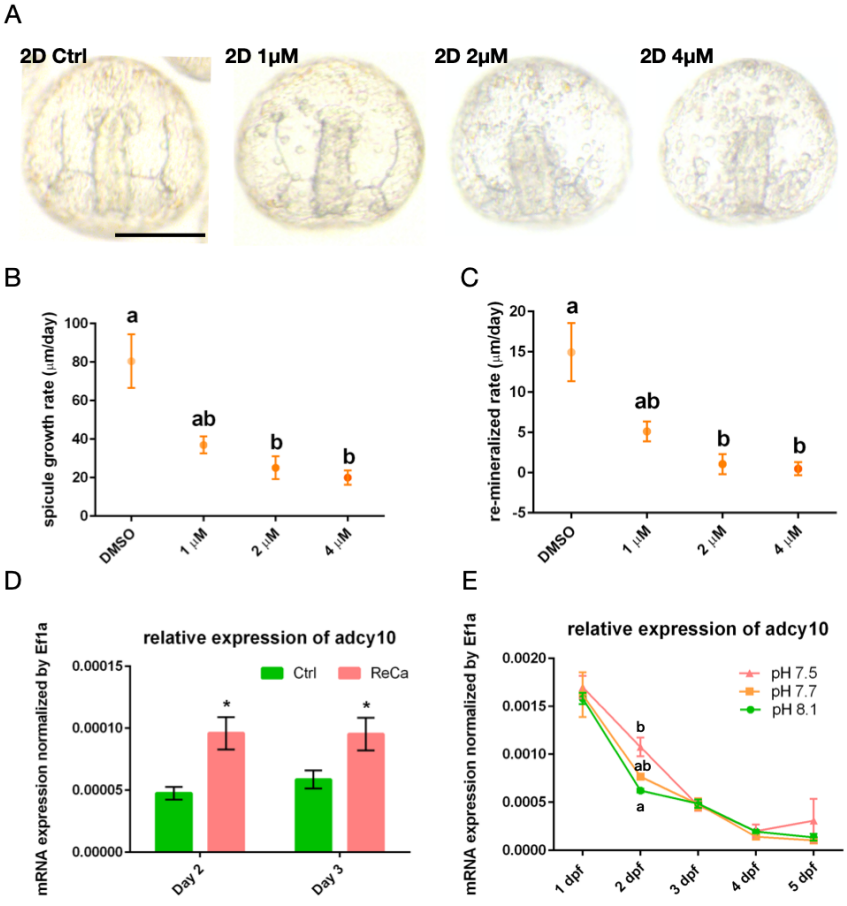

Figure 4 Role of sAC activity for the calcification process in the sea urchin larva. (A) Representative images of 2 dpf larvae demonstrating the effects of the sAC inhibitor, KH7 on the spicule development. Scale bar = 100 μm. (B) Growth rate of spicules (μm/day) in 2 dpf to 4 dpf sea urchin larvae treated with 0, 1, 2, or 4 μM KH7. N = 3, One-way ANOVA: $P<0.05$, Turkey's test. (C) Effect of different concentrations of KH7 on the skeleton re-mineralization rate after the decalcification treatment. N = 3, One-way ANOVA: $P<0.05$, Turkey's test. (D) Transcription levels of *adcy10* in control (Ctrl) and re-mineralization (ReCa) larvae. Sampling from 2 day to 3 days of recovering from the decalcification treatment. N = 5-6, Student's T-test: $P<0.05$. (E) The mRNA level of $_{su}$sAC in 1-5 dpf larvae treated with pH 8.1 SW (green), pH 7.7 SW (orange), or pH 7.5 SW (pink). N = 3, Values are presented as mean ± SEM. Statistical differences were analyzed by One-way ANOVA: $P<0.05$, Turkey's test.

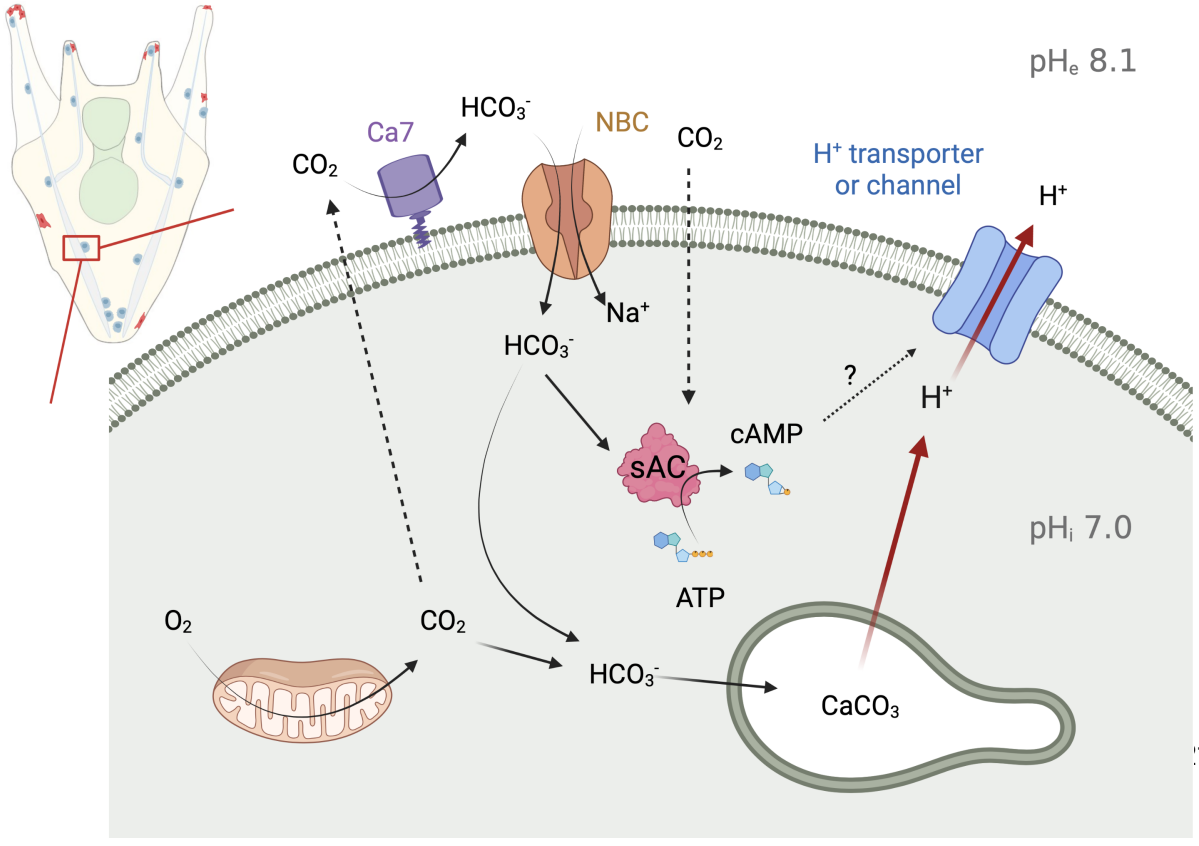

Figure 5 Proposed model for $_{su}$sAC-dependent coordination of sea urchin PMC pHi regulation and biomineralization. During active PMC biomineralization, $_{su}$sAC is stimulated by an increase in cytosolic HCO_3^- levels resulting from NBC-mediated HCO_3^- import, which was contributed by Cara7 (CA7) converting metabolic CO_2. The subsequent $_{su}$sAC-dependent increase in cAMP regulates the activity of downstream effector H^+-transporting proteins; the most likely candidates include Otop2L, VHA, and NHE. The effectors were triggered by cAMP through an uncertain stimulation pathway. Figure was created with BioRender.com.

References

1. **Knoll AH**. Biomineralization and Evolutionary History. *Rev Mineral Geochemistry* 54: 329–356, 2003. doi: 10.2113/0540329.
2. **Sikes CS**, **Okazaki K**, **Fink RD**. Respiratory CO2 and the supply of inorganic carbon for calcification of sea urchin embryos. *Comp Biochem Physiol -- Part A Physiol* 70: 285–291, 1981. doi: 10.1016/0300-9629(81)90181-X.
3. **Sevilgen DS**, **Venn AA**, **Hu MY**, **Tambutté E**, **De Beer D**, **Planas-Bielsa V**, **Tambutté S**. Full in vivo characterization of carbonate chemistry at the site of calcification in corals. *Sci Adv* 5: 1–10, 2019. doi: 10.1126/sciadv.aau7447.
4. **Ramesh K**, **Hu MY**, **Thomsen J**, **Bleich M**, **Melzner F**. Mussel larvae modify calcifying fluid carbonate chemistry to promote calcification. *Nat Commun* 8: 1–8, 2017. doi: 10.1038/s41467-017-01806-8.

5. **Jurikova H**, **Liebetrau V**, **Gutjahr M**, **Rollion-Bard C**, **Hu MY**, **Krause S**, **Henkel D**, **Hiebenthal C**, **Schmidt M**, **Laudien J**, **Eisenhauer A**. Boron isotope systematics of cultured brachiopods: Response to acidification, vital effects and implications for palaeo-pH reconstruction. *Geochim Cosmochim Acta* 248: 370–386, 2019. doi: 10.1016/j.gca.2019.01.015.
6. **Hu MY**, **Petersen I**, **Chang WW**, **Blurton C**, **Stumpp M**. Cellular bicarbonate accumulation and vesicular proton transport promote calcification in the sea urchin larva: Mechanism of skeleton calcification. *Proc R Soc B Biol Sci* 287, 2020. doi: 10.1098/rspb.2020.1506.
7. **Kwan GT**, **Tresguerres M**. Elucidating the acid-base mechanisms underlying otolith overgrowth in fish exposed to ocean acidification. *Sci Total Environ* 823: 153690, 2022. doi: https://doi.org/10.1016/j.scitotenv.2022.153690.
8. **Lacruz RS**, **Nanci A**, **Kurtz I**, **Wright JT**, **Paine ML**. Regulation of pH during amelogenesis. *Calcif Tissue Int* 86: 91–103, 2010. doi: 10.1007/s00223-009-9326-7.
9. **Taylor AR**, **Chrachri A**, **Wheeler G**, **Goddard H**, **Brownlee C**. A Voltage-Gated H^+ Channel Underlying pH Homeostasis in Calcifying Coccolithophores. *PLoS Biol* 9: e1001085, 2011. doi: 10.1371/journal.pbio.1001085.
10. **Beniash E**, **Aizenberg J**, **Addadi L**, **Weiner S**. Amorphous calcium carbonate transforms into calcite during sea urchin larval spicule growth. *Proc R Soc B Biol Sci* 264: 461–465, 1997. doi: 10.1098/rspb.1997.0066.
11. **Vidavsky N**, **Addadi S**, **Mahamid J**, **Shimoni E**, **Ben-Ezra D**, **Shpigel M**, **Weiner S**, **Addadi L**. Initial stages of calcium uptake and mineral deposition in sea urchin embryos. *Proc Natl Acad Sci* 111: 39–44, 2014. doi: 10.1073/pnas.1312833110.
12. **Liu L**, **Schlesinger PH**, **Slack NM**, **Friedman PA**, **Blair HC**. High capacity Na^+/H^+ exchange activity in mineralizing osteoblasts. *J Cell Physiol* 226: 1702–1712, 2011. doi: 10.1002/jcp.22501.
13. **Stumpp M**, **Hu MY**, **Melzner F**, **Gutowska MA**, **Dorey N**, **Himmerkus N**, **Holtmann WC**, **Dupont ST**, **Thorndyke MC**, **Bleich M**. Acidified seawater impacts sea urchin larvae pH

regulatory systems relevant for calcification. *Proc Natl Acad Sci U S A* 109: 18192–18197, 2012. doi: 10.1073/pnas.1209174109.

14. **Hu MY**, **Yan JJ**, **Petersen I**, **Himmerkus N**, **Bleich M**, **Stumpp M**. A SLC4 family bicarbonate transporter is critical for intracellular pH regulation and biomineralization in sea urchin embryos. *Elife* 7: 1–17, 2018. doi: 10.7554/eLife.36600.
15. **Chang WW**, **Matt A**, **Schewe M**, **Musinszki M**, **Grüssel S**, **Brandenburg J**, **Garfield D**, **Bleich M**, **Baukrowitz T**, **Hu MY**. An otopetrin family proton channel promotes cellular acid efflux critical for biomineralization in a marine calcifier. *Proc Natl Acad Sci* 118: e2101378118, 2021. doi: 10.1073/pnas.2101378118.
16. **Matt AS**, **Chang WW**, **Hu MY**. Extracellular carbonic anhydrase activity promotes a carbon concentration mechanism in metazoan calcifying cells. *Proc Natl Acad Sci U S A* 119: 1–11, 2022. doi: 10.1073/pnas.2203904119.
17. **Kwan GT**, **Smith TR**, **Tresguerres M**. Immunological characterization of two types of ionocytes in the inner ear epithelium of Pacific Chub Mackerel (Scomber japonicus). *J Comp Physiol B Biochem Syst Environ Physiol* 190: 419–431, 2020. doi: 10.1007/s00360-020-01276-3.
18. **Barott KL**, **Venn AA**, **Thies AB**, **Tambutté S**, **Tresguerres M**. Regulation of coral calcification by the acid-base sensing enzyme soluble adenylyl cyclase. *Biochem Biophys Res Commun* 525: 576–580, 2020. doi: 10.1016/j.bbrc.2020.02.115.
19. **Tresguerres M**, **Parks SK**, **Salazar E**, **Levin LR**, **Goss GG**, **Buck J**. Bicarbonate-sensing soluble adenylyl cyclase is an essential sensor for acid/base homeostasis. *Proc Natl Acad Sci U S A* 107: 442–447, 2010. doi: 10.1073/pnas.0911790107.
20. **Tresguerres M**, **Levin LR**, **Buck J**. Intracellular cAMP signaling by soluble adenylyl cyclase. *Kidney Int* 79: 1277–1288, 2011. doi: 10.1038/ki.2011.95.
21. **Kobayashi M**, **Buck J**, **Levin LR**. Conservation of functional domain structure in bicarbonate-regulated “soluble” adenylyl cyclases in bacteria and eukaryotes. *Dev Genes Evol* 214: 503–509, 2004. doi: 10.1007/s00427-004-0432-2.

22. **Chen Y**, **Cann MJ**, **Litvin TN**, **Iourgenko V**, **Sinclair ML**, **Levin LR**, **Buck J**. Soluble Adenylyl Cyclase as an Evolutionarily Conserved Bicarbonate Sensor. *Science (80-)* 289: 625–628, 2000. doi: 10.1126/science.289.5479.625.
23. **Tresguerres M**. SAC from aquatic organisms as a model to study the evolution of acid/base sensing. *Biochim Biophys Acta - Mol Basis Dis* 1842: 2629–2635, 2014. doi: 10.1016/j.bbadis.2014.06.021.
24. **Tresguerres M**, **Clifford AM**, **Harter TS**, **Roa JN**, **Thies AB**, **Yee DP**, **Brauner CJ**. Evolutionary links between intra- and extracellular acid–base regulation in fish and other aquatic animals. *J Exp Zool Part A Ecol Integr Physiol* 333: 449–465, 2020. doi: 10.1002/jez.2367.
25. **Roa JN**, **Tresguerres M**. Soluble adenylyl cyclase is an acid-base sensor in epithelial base-secreting cells. *Am J Physiol - Cell Physiol* 311: C340–C349, 2016. doi: 10.1152/ajpcell.00089.2016.
26. **Roa JN**, **Tresguerres M**. Bicarbonate-sensing soluble adenylyl cyclase is present in the cell cytoplasm and nucleus of multiple shark tissues. *Physiol Rep* 5: 1–14, 2017. doi: 10.14814/phy2.13090.
27. **Salmerón C**, **Harter TS**, **Kwan GT**, **Roa JN**, **Blair SD**, **Rummer JL**, **Shiels HA**, **Goss GG**, **Wilson RW**, **Tresguerres M**. Molecular and biochemical characterization of the bicarbonate-sensing soluble adenylyl cyclase from a bony fish, the rainbow trout Oncorhynchus mykiss. *Interface Focus* 11: 20200026, 2022. doi: 10.1098/rsfs.2020.0026.
28. **Roa JN**, **Munévar CL**, **Tresguerres M**. Feeding induces translocation of vacuolar proton ATPase and pendrin to the membrane of leopard shark (Triakis semifasciata) mitochondrion-rich gill cells. *Comp Biochem Physiol Part A Mol Integr Physiol* 174: 29–37, 2014. doi: https://doi.org/10.1016/j.cbpa.2014.04.003.
29. **Pastor-Soler NM**, **Hallows KR**, **Smolak C**, **Gong F**, **Brown D**, **Breton S**. Alkaline pH- And cAMP-induced V-ATPase membrane accumulation is mediated by protein kinase a in epididymal clear cells. *Am J Physiol - Cell Physiol* 294: 488–494, 2008. doi: 10.1152/ajpcell.00537.2007.

30. **Gong F**, **Alzamora R**, **Smolak C**, **Li H**, **Naveed S**, **Neumann D**, **Hallows KR**, **Pastor-Soler NM**. Vacuolar H^+-ATPase apical accumulation in kidney intercalated cells is regulated by PKA and AMP-activated protein kinase. *Am J Physiol - Ren Physiol* 298: 1162–1169, 2010. doi: 10.1152/ajprenal.00645.2009.
31. **Carvalho ESM**, **Gregório SF**, **Power DM**, **Canário AVM**, **Fuentes J**. Water absorption and bicarbonate secretion in the intestine of the sea bream are regulated by transmembrane and soluble adenylyl cyclase stimulation. *J Comp Physiol B Biochem Syst Environ Physiol* 182: 1069–1080, 2012. doi: 10.1007/s00360-012-0685-4.
32. **Buck J**, **Sinclair ML**, **Schapal L**, **Cann MJ**, **Levin LR**. Cytosolic adenylyl cyclase defines a unique signaling molecule in mammals. *Proc Natl Acad Sci U S A* 96: 79–84, 1999. doi: 10.1073/pnas.96.1.79.
33. **Nomura M**, **Beltra C**, **Darszon A**, **Vacquier VD**. A soluble adenylyl cyclase from sea urchin spermatozoa B. 353: 231–238, 2005. doi: 10.1016/j.gene.2005.04.034.
34. **Beltrán C**, **Vacquier VD**, **Moy G**, **Chen Y**, **Buck J**, **Levin LR**, **Darszon A**. Particulate and soluble adenylyl cyclases participate in the sperm acrosome reaction. *Biochem Biophys Res Commun* 358: 1128–1135, 2007. doi: 10.1016/j.bbrc.2007.05.061.
35. **Shipp LE**, **Hill RZ**, **Moy GW**, **Gökirmak T**, **Hamdoun A**. Abcc5 is required for camp-mediated hindgut invagination in sea urchin embryos. *Dev* 142: 3537–3548, 2015. doi: 10.1242/dev.126144.
36. **Moreno B**, **DiCorato A**, **Park A**, **Mobilia K**, **Knapp R**, **Bleher R**, **Wilke C**, **Alvares K**, **Joester D**. Chapter 13 - Culture of and experiments with sea urchin embryo primary mesenchyme cells. In: *Echinoderms, Part A*, edited by Foltz KR, Hamdoun ABT-M in CB. Academic Press, 2019, p. 293–330.
37. **Rafiq K**, **Shashikant T**, **Mcmanus CJ**, **Ettensohn CA**, **Rafiq K**, **Shashikant T**, **Mcmanus CJ**, **Ettensohn CA**. Erratum to Genome-wide analysis of the skeletogenic gene regulatory network of sea urchins (Development, (2014), 141, (950-961), 10.1242/dev.105585). *Dev* 141: 2542, 2014. doi: 10.1242/dev.112763.

38. **Smith J**, **Davidson EH**. A new method, using cis-regulatory control, for blocking embryonic gene expression. *Dev Biol* 318: 360–365, 2008. doi: 10.1016/j.ydbio.2008.02.056.
39. **Tresguerres M**, **Salmerón C**. Chapter Seventeen - Molecular, Enzymatic, and Cellular Characterization of Soluble Adenylyl Cyclase From Aquatic Animals. In: *Marine Enzymes and Specialized Metabolism - Part B*, edited by Moore BSBT-M in E. Academic Press, 2018, p. 525–549.
40. **Salmerón C**, **Harter TS**, **Kwan GT**, **Roa JN**, **Blair SD**, **Rummer JL**, **Shiels HA**, **Goss GG**, **Wilson RW**, **Tresguerres M**. Molecular and biochemical characterization of the bicarbonate-sensing soluble adenylyl cyclase from a bony fish, the rainbow trout Oncorhynchus mykiss. *Interface Focus* 11, 2021. doi: 10.1098/rsfs.2020.0026.
41. **Chen X**, **Baumlin N**, **Buck J**, **Levin LR**, **Fregien N**, **Salathe M**. A soluble adenylyl cyclase form targets to axonemes and rescues beat regulation in soluble adenylyl cyclase knockout mice. *Am J Respir Cell Mol Biol* 51: 750–760, 2014. doi: 10.1165/rcmb.2013-0542OC.
42. **Espejo MS**, **Orlowski A**, **Ibañez AM**, **Di Mattía RA**, **Velásquez FC**, **Rossetti NS**, **Ciancio MC**, **De Giusti VC**, **Aiello EA**. The functional association between the sodium/bicarbonate cotransporter (NBC) and the soluble adenylyl cyclase (sAC) modulates cardiac contractility. *Pflugers Arch Eur J Physiol* 472: 103–115, 2020. doi: 10.1007/s00424-019-02331-x.
43. **Wilson CM**, **Roa JN**, **Cox GK**, **Tresguerres M**, **Farrell AP**. Introducing a novel mechanism to control heart rate in the ancestral Pacific hagfish. *J Exp Biol* 219: 3227–3236, 2016. doi: 10.1242/jeb.138198.
44. **Lo M**, **Shahriari A**, **Roa JN**, **Tresguerres M**, **Farrell AP**. Differential effects of bicarbonate on severe hypoxia- and hypercapnia-induced cardiac malfunctions in diverse fish species. *J Comp Physiol B Biochem Syst Environ Physiol* 191: 113–125, 2021. doi: 10.1007/s00360-020-01324-y.
45. **Barott KL**, **Perez SO**, **Linsmayer LB**, **Tresguerres M**. Differential localization of ion transporters suggests distinct cellular mechanisms for calcification and photosynthesis

between two coral species. *Am J Physiol - Regul Integr Comp Physiol* 309: R235–R246, 2015. doi: 10.1152/ajpregu.00052.2015.

46. **Tresguerres M**, **Barott KL**, **Barron ME**, **Deheyn DD**, **Kline DI**, **Linsmayer LB**. Cell Biology of Reef-Building Corals: Ion Transport, Acid/Base Regulation, and Energy Metabolism BT - Acid-Base Balance and Nitrogen Excretion in Invertebrates: Mechanisms and Strategies in Various Invertebrate Groups with Considerations of Challenges Ca. In: , edited by Weihrauch D, O'Donnell M. Cham: Springer International Publishing, 2017, p. 193–218.
47. **Yin K**, **Paine ML**. Bicarbonate Transport During Enamel Maturation. *Calcif Tissue Int* 101: 457–464, 2017. doi: 10.1007/s00223-017-0311-2.
48. **Thouverey C**, **Malinowska A**, **Balcerzak M**, **Strzelecka-Kiliszek A**, **Buchet R**, **Dadlez M**, **Pikula S**. Proteomic characterization of biogenesis and functions of matrix vesicles released from mineralizing human osteoblast-like cells. *J Proteomics* 74: 1123–1134, 2011. doi: 10.1016/j.jprot.2011.04.005.
49. **Barott KL**, **Barron ME**, **Tresguerres M**. Identification of a molecular pH sensor in coral. *Proc R Soc B Biol Sci* 284: 1–8, 2017. doi: 10.1098/rspb.2017.1769.
50. **Ichikawa S**, **Koller DL**, **Curry LR**, **Lai D**, **Xuei X**, **Edenberg HJ**, **Hui SL**, **Peacock M**, **Foroud T**, **Econs MJ**. Association of adenylate cyclase 10 (ADCY10) polymorphisms and bone mineral density in healthy adults. *Calcif Tissue Int* 84: 97–102, 2009. doi: 10.1007/s00223-008-9200-z.
51. **Shi W**, **Gao Y**, **Wang Y**, **Zhou J**, **Wei Z**, **Ma X**, **Ma H**, **Xian CJ**, **Wang J**, **Chen K**. The flavonol glycoside icariin promotes bone formation in growing rats by activating the cAMP signaling pathway in primary cilia of osteoblasts. *J Biol Chem* 292: 20883–20896, 2017. doi: 10.1074/jbc.M117.809517.
52. **Stumpp M**, **Hu M**, **Casties I**, **Saborowski R**, **Bleich M**, **Melzner F**, **Dupont S**. Digestion in sea urchin larvae impaired under ocean acidification. *Nat Clim Chang* 3: 1044–1049, 2013. doi: 10.1038/nclimate2028.

53. **Pennington JT**, **Strathmann RR**. Consequences of the calcite skeletons of planktonic echinoderm larvae for orientation, swimming, and shape. *Biol Bull* 179: 121–133, 1990. doi: 10.2307/1541746.

54. **Kumar S**, **Stecher G**, **Li M**, **Knyaz C**, **Tamura K**. MEGA X: Molecular evolutionary genetics analysis across computing platforms. *Mol Biol Evol* 35: 1547–1549, 2018. doi: 10.1093/molbev/msy096.

55. **McClay DR**. Methods for Embryo Dissociation and Analysis of Cell Adhesion. In: *Development of Sea Urchins, Ascidians, and Other Invertebrate Deuterostomes: Experimental Approaches*. Academic Press, 2004, p. 311–329.

56. **Arshinoff BI**, **Cary GA**, **Karimi K**, **Foley S**, **Agalakov S**, **Delgado F**, **Lotay VS**, **Ku CJ**, **Pells TJ**, **Beatman TR**, **Kim E**, **Andrew Cameron R**, **Vize PD**, **Telmer CA**, **Croce JC**, **Ettensohn CA**, **Hinman VF**. Echinobase: Leveraging an extant model organism database to build a knowledgebase supporting research on the genomics and biology of echinoderms. *Nucleic Acids Res* 50: D970–D979, 2022. doi: 10.1093/nar/gkab1005.

57. **Butler A**, **Hoffman P**, **Smibert P**, **Papalexi E**, **Satija R**. Integrating single-cell transcriptomic data across different conditions, technologies, and species. *Nat Biotechnol* 36: 411–420, 2018. doi: 10.1038/nbt.4096.

58. **Stuart T**, **Butler A**, **Hoffman P**, **Hafemeister C**, **Papalexi E**, **Mauck WM**, **Hao Y**, **Stoeckius M**, **Smibert P**, **Satija R**. Comprehensive Integration of Single-Cell Data. *Cell* 177: 1888-1902.e21, 2019. doi: 10.1016/j.cell.2019.05.031.

59. **Hess KC**, **Jones BH**, **Marquez B**, **Chen Y**, **Ord TS**, **Kamenetsky M**, **Miyamoto C**, **Zippin JH**, **Kopf GS**, **Suarez SS**, **Levin LR**, **Williams CJ**, **Buck J**, **Moss SB**. The “soluble” adenylyl cyclase in sperm mediates multiple signaling events required for fertilization. *Dev Cell* 9: 249–259, 2005. doi: 10.1016/j.devcel.2005.06.007.

60. **Körschen HG**, **Hamzeh H**, **Pascal R**, **Alvarez L**, **Bönigk W**, **Kaur N**, **Levin LR**. External fertilization is orchestrated by a pH-regulated soluble adenylyl cyclase controlling sperm motility and chemotaxis. doi: 10.1101/2021.06.18.448929.

Supplementary materials

Figure S1 The graphic summary of SRA database BLAST results. Full-length *adcy10* mRNA sequence (NM_001025209.1) was blast to transcriptome of control (SRX366892) and Alx1 morphants (SRX385939). RNA sequencing reads matched with input sequences were labeled by color blocks.

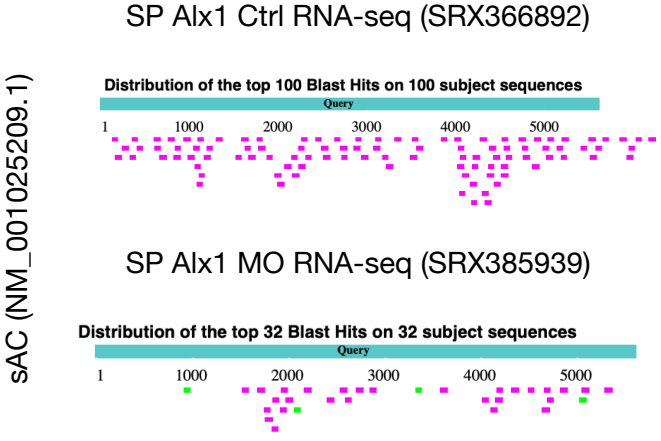

Table S1 The primer sequences of RT-qPCR a

	Gene	Primer sequence	product size (bp)	Note
hybridization probe	**adcy10 (LOC574069)**	F-CGGCTTTCGACTGGAGCTTA	764	
		R-CCTGCATCACTCACACCCTT		
qPCR primers	**adcy10 (LOC574069)**	F-GCAGGCGATGCTTTTCTAGC	184	
		R-CTATGGTCGTGACTCGGACG		
	ef1a (LOC548620)	F-CCGACCTTGGAAAGGGATCG	194	
		R-ACAGTCGGCCTGTGAGGTTC		

nalysis and hybridization probe cloning.